Discrete element model study into effects of particle shape on backfill response to cyclic loading behind an integral bridge abutment

S. Ravjee[1,*], S.W. Jacobsz[1], D.N. Wilke[2,], N. Govender[3,4]

[1].Department of Civil Engineering, University of Pretoria, Pretoria, South Africa

[2.]Department of Mechanical Engineering, University of Pretoria, Pretoria, South Africa

[3].Department of Chemical and Process Engineering, University of Surrey, Surrey, UK

[4].Research Center Pharmaceutical Engineering, Graz, Austria

*Correspondence to: Sachin Ravjee. sachin.ravjee@aurecongroup.com

Email addresses:
Schalk Willem Jacobsz. sw.jacobsz@up.ac.za
Daniel Nicolas Wilke. nico.wilke@up.ac.za
Nicolin Govender. n.govender@surrey.ac.uk

Abstract: The discrete element method, implemented in a modular GPU based framework that supports polyhedral shaped particles (Blaze-DEM), was used to investigate effects of particle shape on backfill response behind integral bridge abutments during temperature-induced displacement cycles. The rate and magnitude of horizontal stress build-up were found to be strongly related to particle sphericity. The stress build-up in particles of high sphericity was gradual and related to densification extending relatively far from the abutment. With increasing angularities, densification was localised near the abutment, but larger and more rapid stress build-up occurred, supported by particle reorientation and interlock developing further away.

Keywords: *Discrete element method (DEM), integral bridge abutments, particle shape, sphericity*

1. Introduction

Over the past 30 years, the disadvantages of using expansion joints and bearings in conventional bridges have become progressively more apparent. These joints and bearings are expensive to purchase, install, repair and maintain and are known to have relatively short lifespans [1]. The inevitable need for the replacement of the expansion joints and bearings results in traffic disruptions and cost implications. An increase in longitudinal deck loading may occur should these joints and bearings not be maintained or replaced when necessary. This may consequently cause overstressing and damage to occur in the weaker bridge components [2,3].

Integral bridges have been designed to eliminate the problems associated with expansion joints and bearings. These bridges are designed without joints or bearings where the abutments are connected to the superstructure. The deck and abutments can, therefore, be viewed as a single structural unit. Thus, the problems associated with the use of joints and bearings in conventional bridges are eliminated. The use of integral bridges simplifies the construction process, reduces maintenance costs, removes the cost of movement joints and bearings and provides greater earthquake resistance [4].

A problem that arises with integral bridges is related to the daily and seasonal temperature variations experienced by the deck. Since there are no joints or bearings present between the superstructure and the abutments, there is an integral connection between them. This means that when the deck either expands or contracts due to temperature variations, the abutments are forced to move relative to the granular backfill it retains. The abutments move away from the backfill when the deck contracts as a result of a temperature decrease and move towards the backfill when the deck expands as a result of a temperature increase. Therefore, due to the movements of the abutment, the granular backfill retained by the abutments is exposed to temperature-induced cyclic loading [1,5].

Research by Clayton *et al.* [1] and Xu *et al.* [3] have shown that the temperature-induced cyclic loading experienced in the backfill may cause a significant build-up of stresses acting on the abutments as the number of cycles increases, associated with a mechanism of ratcheting from progressive particle interlock. These earth pressures can over time become very large, potentially approaching full passive pressure. Clayton *et al.* [1] and Xu *et al.* [3] investigated effects of backfill particle shape on the build-up of stresses behind integral bridge abutments by means of cyclic triaxial testing and found that particle shapes which support possible interlocking resulted in a larger build-up of horizontal stresses in the granular backfill. The mechanism is associated with a ratcheting action developing over many cycles. The particle shape of the granular backfill retained by integral bridge abutments, therefore, has a considerable effect on the accumulation of the earth pressures acting on the abutment [1,3]. It is for this reason that texts on integral bridge design [6,7] recommend that a limit be placed on the shear strength of materials used as backfill behind abutments to limit the magnitude of lateral earth pressures that can be generated.

The Discrete Element Method (DEM), proposed by Cundall and Strack [8], is a popular computational method which can be used to analyse, design and optimise bulk systems containing granular materials of varying shapes. The particle shape and type of particle shape approximation in DEM analyses play a significant role in the results of the simulations. For computational reasons, DEM analyses have traditionally been carried out using spherical particles, with more complex forms sometimes generated by using sphere clumps. However, the use of polyhedral shaped particles, more closely resembling actual particle shapes, results in a more accurate representation of actual material behaviour as opposed to particles generated from sphere-clumps [9–12].

In this study, DEM modelling was used within Blaze-DEM, a research code developed at the University of Pretoria, to investigate the effect of granular particle shape on the response of backfill retained by a model bridge abutment at micro-mechanical level. Backfill response modes investigated were densification, lateral stress build-up and particle reorientation in the backfill during cyclic rotation of the bridge abutment. Blaze-DEM is a high-performance graphics processing unit (GPU) based framework which supports the simulation of spherical, as well as convex and non-convex polyhedra [13].

2. Blaze-DEM

Blaze-DEM is a soft particle DEM simulation environment optimised for the parallel architecture of the general purpose GPU (GPGPU) [13]. Particle contact is estimated using collision detection algorithms within an explicit time integration scheme to estimate the contact volume overlap for convex and non-convex polyhedral shaped particles, as well as overlap distance for spherical particles [14]. The framework offers high-level computational performance for orders more particles compared to what can be simulated on commercial DEM packages that utilise multi-core central processing units (CPUs). The limited number

of cores and threads on CPUs restrict the number of particles that can be simulated within a reasonable time frame [15].

The multicore CPU allows for task parallelism, i.e. each core can conduct a separate task that is performed across the elements of the same or different datasets. However, the limited number of cores available on the CPU limits the number of threads that can be executed concurrently as depicted in Figure 1. Also, as illustrated, the CPU performance is effectively the same when considering the simpler single instruction stream multiple data stream (SIMD) data parallelism task. Consider Table 1, where a 6 core CPU with multi-threading allows for 24 threads to run concurrently per clock cycle. In turn, the GPU allows for data parallelism, i.e. streaming multi-processors (SM) can efficiently solve thousands of threads concurrently to perform the same task across the elements of a dataset [10], as depicted in Figure 1. This is an extension of SIMD to single instruction stream multiple threads (SIMT). Consider again Table 1. The GTX 1080 graphics processor has 20 SMs, each that can run 2 048 threads concurrently, allowing for 40 960 threads to run concurrently per clock cycle.

Blaze-DEM exploits this massively parallel paradigm of the GPU to achieve an elevated level of computational performance [10] when solving DEM problems, since a number of DEM computations per time-step can be cast and solved efficiently using SIMT.

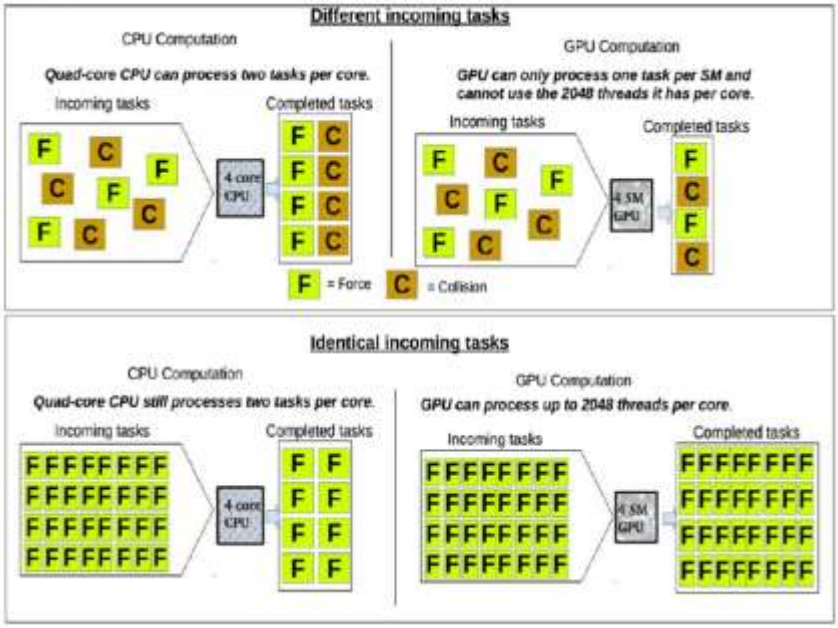

Fig. 1. Comparison of advantages between CPU and GPU [13]

Since Blaze-DEM is a research code, results obtained from it have been extensively validated against experimental results and validated CPU DEM codes. These validations involved mill charge simulations with spheres [16], as well hopper flow tests with spherical and polyhedral shaped particles [10,14]. It was concluded that the GPU and Blaze-DEM are well suited for these DEM analyses [13,15,16]. In this study, the results from Blaze-DEM were validated by performing a software comparison against the results from the commercial code of Siemens PLM, STAR-CCM+ [17]. Two separate computers were used for the simulations with the two software packages, with the processor specifications for each computer summarised in Table 1. The results from the software comparison are shown in Section 4.

Table 1 Comparison of processing unit specifications used for STAR-CCM+ and Blaze-DEM simulations

Component	STAR-CCM+ processing unit	Blaze-DEM processing unit
Processing unit	CPU	GPU
Processing unit make	Intel	GIGABYTE
Processing unit model	Core i7-4930K	GeForce GTX 1080 G1
Number of processing units	1	3
Number of cores per unit	6 (12 Threads)	2 560 (40 960 Threads per Cycle)
Base clock frequency	3.40 GHz	1.72 GHz
Boost clock frequency	3.90 GHz	1.86 GHz
Power usage	130 W	180 W
Recommended price in USA	$594.00	$499.00 per GPU

3. DEM modelling

3.1. Integral bridge abutment modelling

To perform the DEM simulations, a model simulating backfill behind an integral bridge abutment was prepared. The model was loosely based on the design of the existing Van Zylspruit integral bridge in South Africa. The bridge is a reinforced concrete, 90 m long, 5 span, fully integral bridge on the N1 motorway between Bloemfontein and Colesberg in central South Africa [18]. Figure 2 shows a photograph of the Van Zylspruit bridge during construction in December 2016. Large imposed deformations would be required to model a 6 m high abutment and backfill with a 90 m long bridge deck. This would mean that a model with a large number of particles would be required in the DEM simulations to model the behaviour realistically. Therefore, to reduce the number of particles, a scaled down 30 m long deck with 2 m high abutments was modelled. The relevant dimensions of the modelled abutment and deck are shown in Figure 3. The figure illustrates the idealised point of rotation of the abutment due to thermal expansion and contraction from temperature variations in the deck, as well as the active and passive loading directions.

The response of the granular backfill behind the abutments to cyclic displacement cycles from temperature variation was modelled using DEM. To further limit the number of particles used in the DEM simulations, the top portion of the backfill adjacent to the abutment was considered in this study (as shown in Figure 3). The DEM particles were injected into a model space with dimensions of 300 mm x 150 mm x 350 mm. The particles were injected in a regular grid pattern from the top of the container with an initial downward velocity of 5 cm/s and velocities of 1 cm/s in the in-plane directions of the grid. The in-plane velocities were applied to randomly distribute the particles within the container, rather than only dropping them vertically. Once the container was filled with the particles, the abutment was cycled 25 times towards and away from the particles to replicate the temperature-induced loading experienced by the backfill of integral bridges, with the centre of rotation as indicated in Figure 3. This was done for each of the six different particle shapes considered in this study as discussed in Section 3.3. A 3D view of the DEM model is illustrated in Figure 4. The figure shows the rotating abutment and the fixed boundaries.

Bloodworth *et al.* [2] reported that there was little evidence that wall friction significantly influences earth pressures behind integral bridge abutments over the range of typical roughness values. Wall roughness was therefore not varied in this study and all model boundaries were subsequently modelled as rough. Bloodworth *et al.* [2] also mentioned that abutment rigidity only accounted for a 10% difference in earth

pressure magnitudes over the typical range of abutment rigidities of integral bridge abutments. Variations in wall rigidity was therefore not investigated in this study and all boundaries were modelled as perfectly rigid.

Fig. 2. Van Zylspruit integral bridge towards end of construction

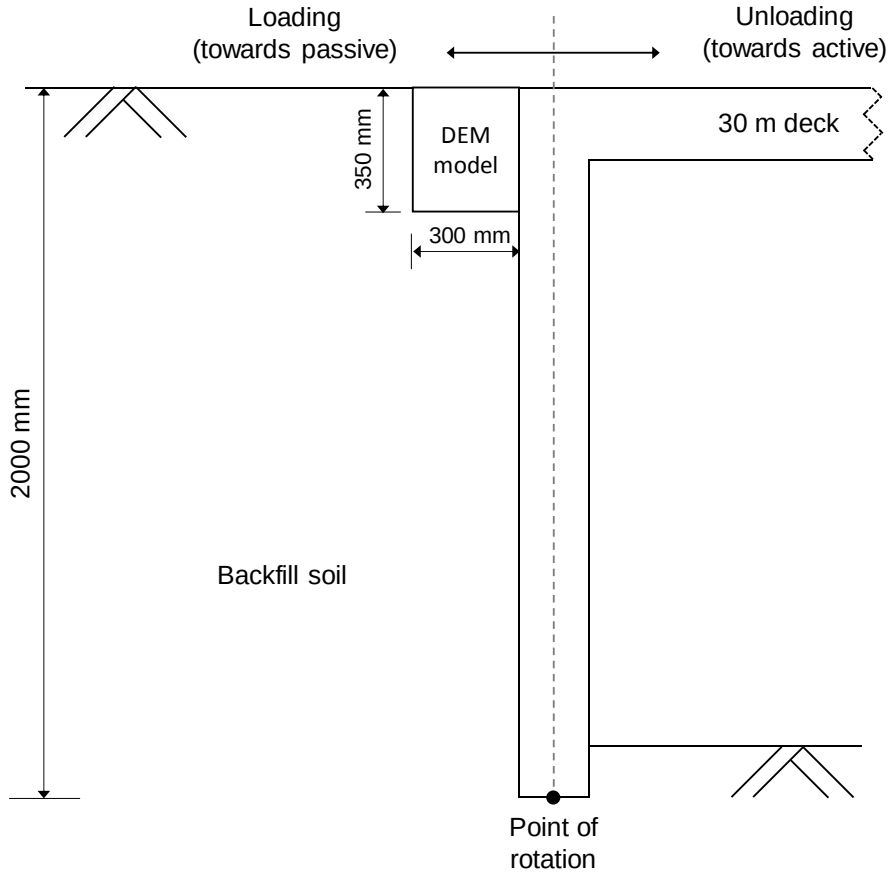

Fig. 3. Schematic of scaled integral bridge abutment showing relevant dimensions

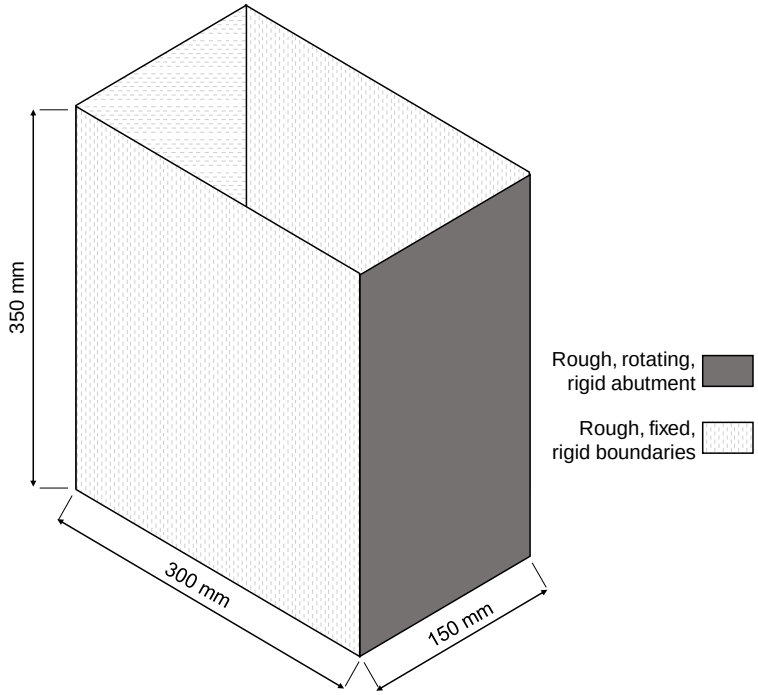

Fig. 4. DEM abutment model

3.2. Imposed deformation

The movements of the bridge deck due to temperature variations were used to determine the angle of rotation of the abutment. This rotation angle was used to cyclically rotate the abutment in the passive and active directions in the DEM analyses. The temperature data from the Van Zylspruit integral bridge [18] and a linear thermal coefficient of expansion of 12 x 10^{-6} °C^{-1} for concrete [3] was used to calculate the expansion of the deck of the bridge. Assuming free expansion, following Roeder [19], and a maximum effective deck temperature variation of 30°C, the integral bridge abutment would be rotated through a total angle of 0.154°, giving half-angles of 0.077° relative to the vertical from the maximum expanded or contracted positions respectively (see Figure 5).

To limit computational cost, it was desired to impose the modelled abutment rotations relatively rapidly while taking care to avoid unrealistic dynamic or inertial effects. Tests were performed, using the model described above with 5 mm diameter spherical particles, to determine the rate of rotation required to model the effect of temperature variations. The lateral earth pressure coefficients were studied for spherical particles with different abutment rotation rates. It was found that a rotation rate of 0.154°/s (0.5 Hz) was slow enough to avoid inertial effects.

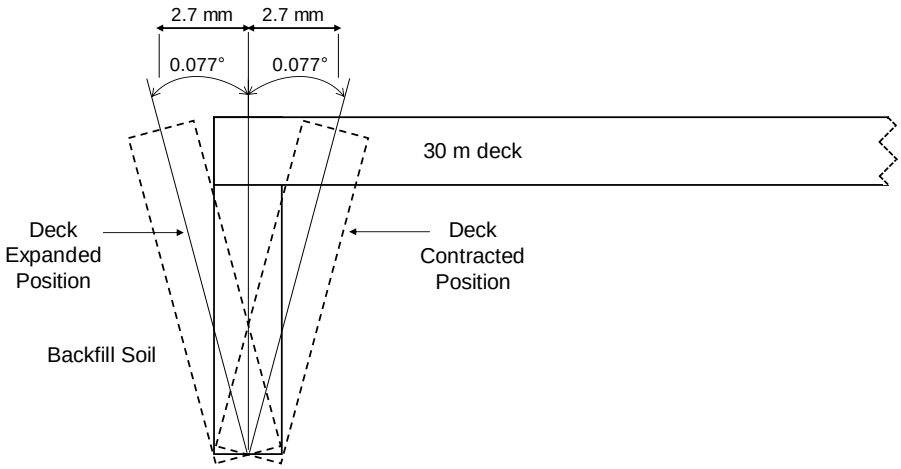

Fig. 5. Representation of the rotation of the abutment

3.3. Particle shape modelling

Various particle shapes were modelled to investigate the effect of granular particle shape on the response of backfill retained by integral bridge abutments. The particle shape plays a significant role in DEM simulations [13] and a range of shapes was therefore used to investigate effects on backfill response resulting from differences in the interaction between particles of different shape. These shapes were spheres and the following convex polyhedral shaped particles: dodecahedrons, tetrahedrons, truncated tetrahedrons, triangular prisms and cubes. These six particle shapes are presented in Figure 6.

The computational time of a DEM simulation is inversely proportional to the size of the particles used [20]. A particle size dependence study was therefore performed to determine the largest size of particles which could be used in the DEM simulations such that the computational times would be the quickest, while minimising unrealistic effect and ensuring that behaviour still represents that of a soil. The lateral earth pressure coefficients were therefore studied for a range of spherical particles sizes. It was found that the size of the particle did not greatly influence the earth pressure coefficients obtained from the simulations, provided that enough particles were used within the model. Larger particle sizes meant that fewer particles were in contact with the abutment and resulted in unstable behaviour, i.e. large variations in the forces acting on the abutment during displacement cycles. It was found that a minimum of approximately 1 000 particles were required to be in contact with the abutment for the lateral earth pressure coefficients to vary relatively smoothly over each displacement cycle. It was found that, using the DEM abutment model from this study, spheres with a diameter of 5 mm resulted in at least 1 000 particles being in contact with the abutment (±100 000 particles in the model). It was therefore decided to use particles with a major dimension of approximately 5 mm in the DEM simulations. Although the sizes of the various shaped particles did vary somewhat, it was found that this was of minor significance as long as a minimum number of approximately 1 000 particles were in contact with the moving model abutment.

To be able to study the effect of different particle shapes used as backfill retained by integral bridge abutments, the particle shapes required classification. The definition of particle sphericity proposed by Wadell [21] is a measure of how closely the shape of a particle approaches that of a mathematically perfect sphere and was found to be a convenient parameter for this study. The sphericities (Figure 7) for the six particle shapes selected for DEM simulations were calculated as follows [21]:

$$\psi = \frac{A_s}{A_p} = \frac{\pi^{\frac{1}{3}}(6V_p)^{\frac{2}{3}}}{A_p}$$

Where:

ψ Sphericity of a particle shape

V_p Volume of a particle shape $[m^3]$

A_p Surface area of a particle shape $[m^2]$

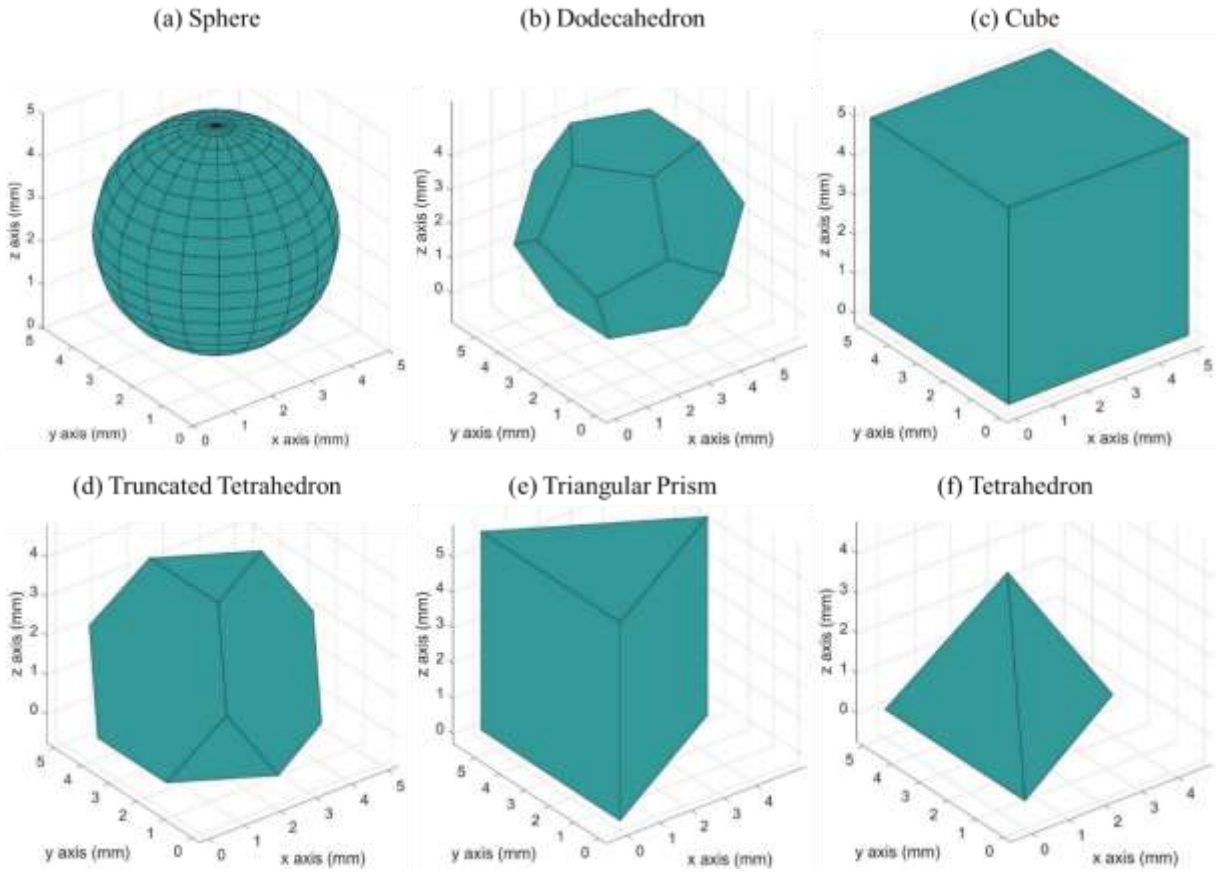

Fig. 6. DEM particle shapes in sequence of decreasing sphericity

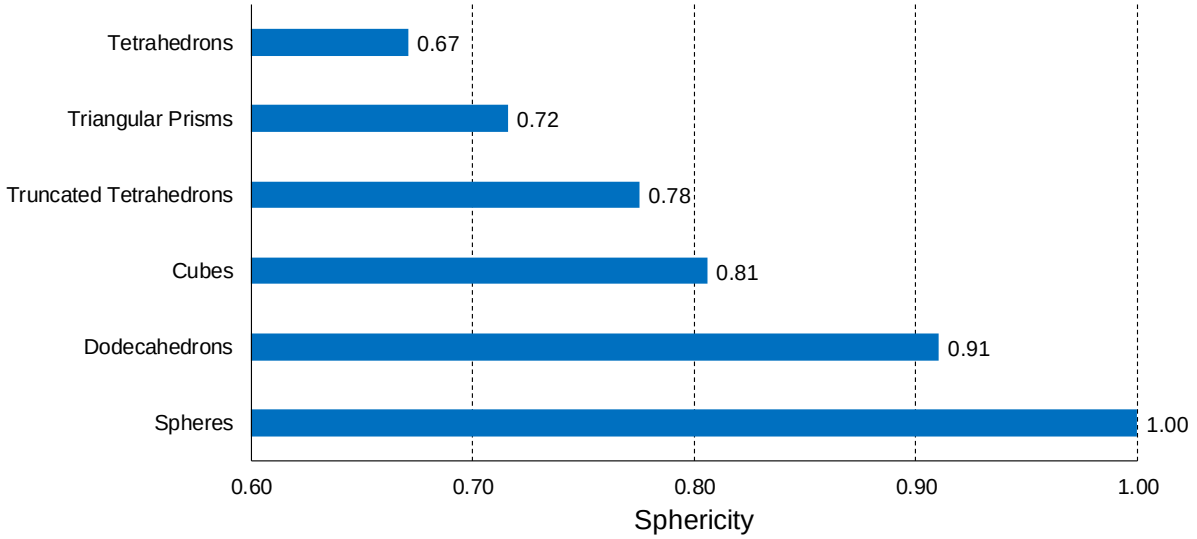

Fig. 7. Sphericities of DEM particle shapes

3.4. Material properties

The material properties used in DEM simulations play a significant role in the accuracy of the results [22]. A number of the parameters were obtained from previous similar work. A particle density of 2 650 kg/m^3 was selected and a particle-wall friction coefficient of 0.70 was obtained from Xu *et al.* [23] who investigated the effects of material properties on granular flow in a silo using DEM simulation. The linear spring-dashpot model [22] was used for the simulations and therefore normal and tangential restitution coefficients were required. Restitution coefficients of 0.50 and 0.60 were used for the normal and tangential directions respectively and a particle-particle friction coefficient of 0.45 was used for each of the six particle shapes considered in this study, similar to work performed by Coetzee [22], who performed a review of literature on the calibration of DEM particles. In the cases of both the spherical and polyhedral particle systems, local rotational damping was applied using a rolling coefficient of 0.001, i.e. the angular rotation was damped using the rolling coefficient so that the angular velocity was decreased by the product of the rolling coefficient and angular velocity in every time step, similar to approaches by Chang *et al.* [24], Tu and Andrade [25] and Sandlin [26].

A time-step of 1×10^{-5} seconds was used for all simulations in Blaze-DEM. This time-step was chosen since it was the largest possible step which resulted in stable particle behaviour between each iteration. Time-steps larger than 1×10^{-5} seconds resulted in erratic particle behaviour and steps smaller than the selected time-step would have resulted in unnecessarily longer computational times.

The computational times of DEM simulations are directly proportional to the square root of the Young's Modulus of the particles [17]. Previous researchers, e.g. Coetzee [20,22], Xu *et al.* [23] and Härtl and Ooi [27] have shown that the theoretically correct Young's Modulus values for DEM particles can be reduced to speed up the computational times of their DEM simulations without detrimentally affecting the results of the analyses. In this study, reduction factors of 10 000, 1 000 and 100 were applied to a theoretical modulus value of 70 GPa, representative of quartz sand, to obtain 7 MPa, 70 MPa and 700 MPa respectively. In the simulations, 140 000 spherical particles, with diameters of 5 mm, were injected into the DEM abutment model shown in Figure 4 and the abutment was rotated once in the active direction and once in the passive direction after which the density with depth distributions were compared to assess the

effect of the modulus reduction. The rotation rate of 0.154°/s and rotation angle of 0.154° resulted in a total simulated time of 2 seconds per cycle. Using the time-step of 1×10^{-5} seconds meant that a total of 200 000 iterations were required for each simulation. Table 2 presents the computational times for the DEM simulations carried out in this study with the various Young's Moduli using Blaze-DEM.

The simulation with the 700 MPa particles completed a full cycle almost eight times faster than the computational time with the 70 GPa particles. The computational times obtained from the 70 MPa and 7 MPa particles provided significantly faster times than the 70 GPa particles, with the 70 MPa particles running 31.8 times faster and the 7 MPa particles over 100 times faster. The time factor of 31.8 obtained from the 70 MPa particles was almost identical to the time factor of 31.6 obtained by Xu *et al.* [23] when applying the same reduction factor to 70 GPa particles. Figure 8 shows a comparison of the computational times for the different Young's Modulus values in Blaze-DEM. The figure highlights the computational benefits of reducing the Young's Modulus.

Table 2 Blaze-DEM computational times for Young's Modulus values

Young's Modulus	Reduction factor	Computational time	Times faster than 70 GPa particles
7 MPa	10 000	2.7 minutes	107.8 ×
70 MPa	1 000	9.2 minutes	31.8 ×
700 MPa	100	37.9 minutes	7.7 ×
70 GPa	1	291.9 minutes	-

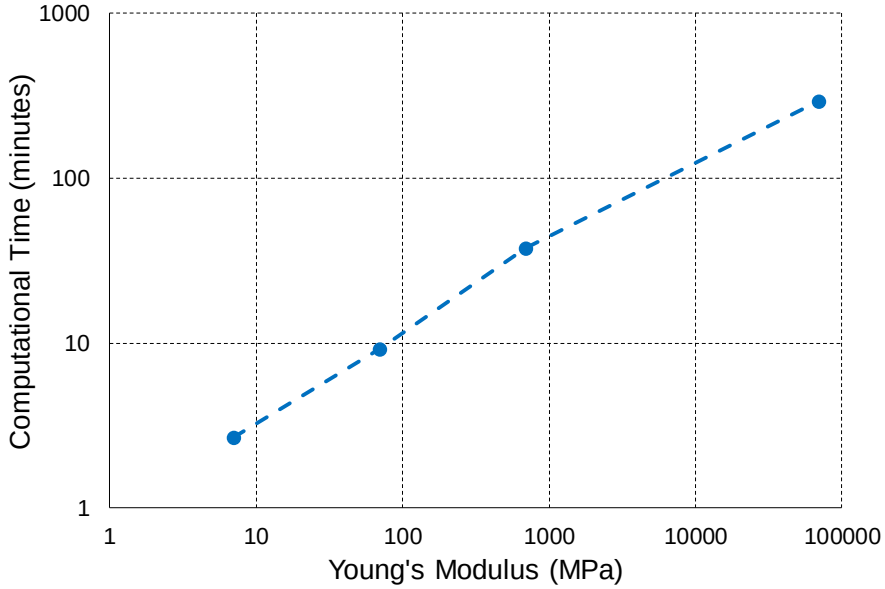

Fig. 8. Computational times for various Young's Modulus values

While the reduction of the Young's Modulus resulted in a major reduction in computational cost, it is essential that the implications of this step on the compressibility of material in the model be considered. As such, the density with depth of material placed behind the DEM model abutment was investigated. The distribution of densities with depth, obtained from the 140 000 particles in Blaze-DEM for the four Young's Modulus values considered, are presented in Figure 9. The figure shows that the 70 MPa and 700 MPa particles yielded densities with depth similar to the 70 GPa particles. However, the 7 MPa particles resulted

in significantly larger densities, particularly near the bottom of the model. These results suggested that the 7 MPa particles experienced unrealistic deformations at the bottom of the model, implying that the particles were too soft to model granular backfill behaviour realistically.
Since the 70 MPa and 700 MPa particles produced comparable results to 70 GPa particles in this study, it was determined that a Young's Modulus of 70 MPa would be the most practical for the DEM simulations. This value would be expected to offer the lowest computational times without significantly compromising the accuracy of the results given the adopted problem geometry.

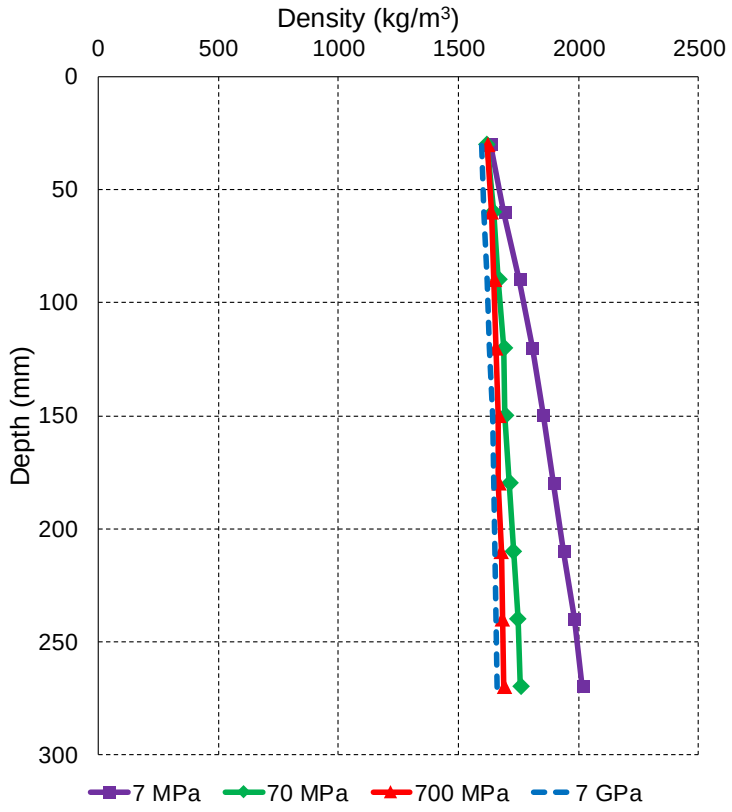

Fig. 9. Blaze-DEM density with depth vs Young's Modulus reduction comparison

4. Software comparison

Blaze-DEM is a recently developed research code and not commercial software. Results of the specific application simulated needed to be verified. A comparison, with selected results presented, was therefore performed between Blaze-DEM and the commercial code developed by Siemens PLM, STAR-CCM+ [17]. This comparison involved filling the DEM abutment model with 90 000 cubic particles and rotating the abutment 25 times in the active and passive directions by the angles mentioned in Section 3.2. Spheres represent the most common DEM particles [20,22] and software packages capable of modelling different shapes are rare [13,14,28]. Therefore, since both STAR-CCM+ and Blaze-DEM offered the capability to model cubes, it was decided to run a comparison using this shape.
The methods used to fill the particles in the containers in the respective software suites differed. The particles were injected in the container in Blaze-DEM, as described in Section 3.1. However, to reduce the

computational times in STAR-CCM+, all 90 000 cubic particles were generated in the first iteration by placing them in a grid across the entire container. Once the particles were generated, they were allowed to settle under only gravitational loads. The different methods of placement were used because of different limitations in both software suites. The differences are considered below.

The simulation required 1 004 hours (41.82 days) of computational time in STAR-CCM+. Blaze-DEM allows the option of performing simulations without a live graphics output, i.e. without displaying the DEM particles while the simulation was performed. The Blaze-DEM simulation performed with a live graphics output required 34.62 hours, whereas the simulation without a live graphics output required only 6.48 hours of computational time, powerfully illustrating the benefits of GPU computing in DEM studies. A presentation of the computational times from the software comparison test is illustrated in Figure 10. All computational times presented exclude the times required to generate or inject the particles, comparing only the time required to model the 25 displacement cycles.

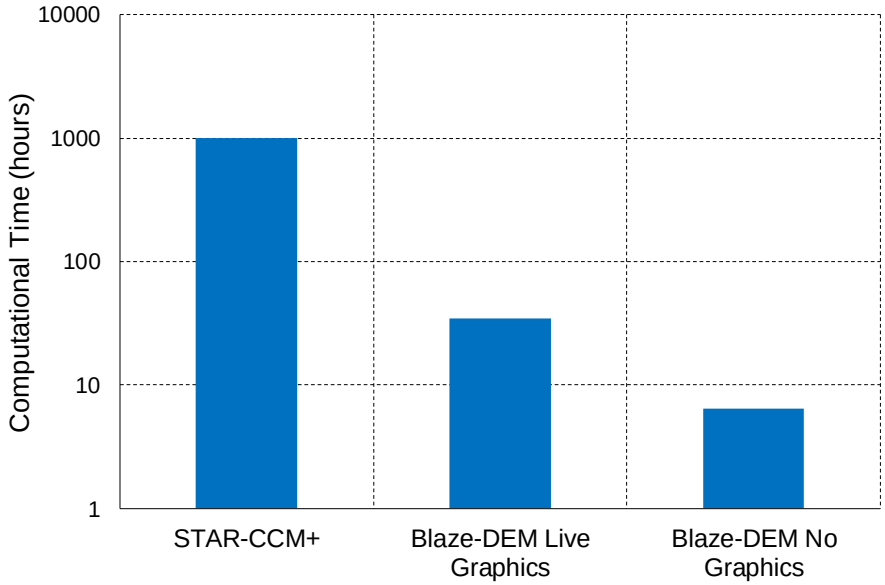

Fig. 10. Software computational time comparison

The bulk densities (Figure 11) and lateral earth pressure coefficients (Figure 12) obtained from the two software packages were analysed. The lateral earth pressure coefficient was calculated by dividing the total horizontal force on the wall by the force calculated by integrating the vertical stress determined from the bulk density distribution with depth over the area of the wall (analogous to the hydrostatic pressure), similar to Kelesoglo and Springman [29]. The comparison of the results showed that there was a slight difference in the initial densities but a more significant difference in the initial earth pressures due to the different injection methods used by the two software packages. Since the particles were injected into the container in Blaze-DEM, a slightly higher initial packing density was obtained, but more significantly, also a different packing structure, causing the more significant difference in lateral earth pressure coefficients. However, after 25 cycles the lateral earth pressure coefficients from both software suites were similar, with Blaze-DEM yielding results over 150 times faster than STAR-CCM+ and almost 30 times faster when using a live graphics output. The investigation using the six different particle shapes was subsequently performed in Blaze-DEM, since performing the simulations in STAR-CCM+ would have been impractical.

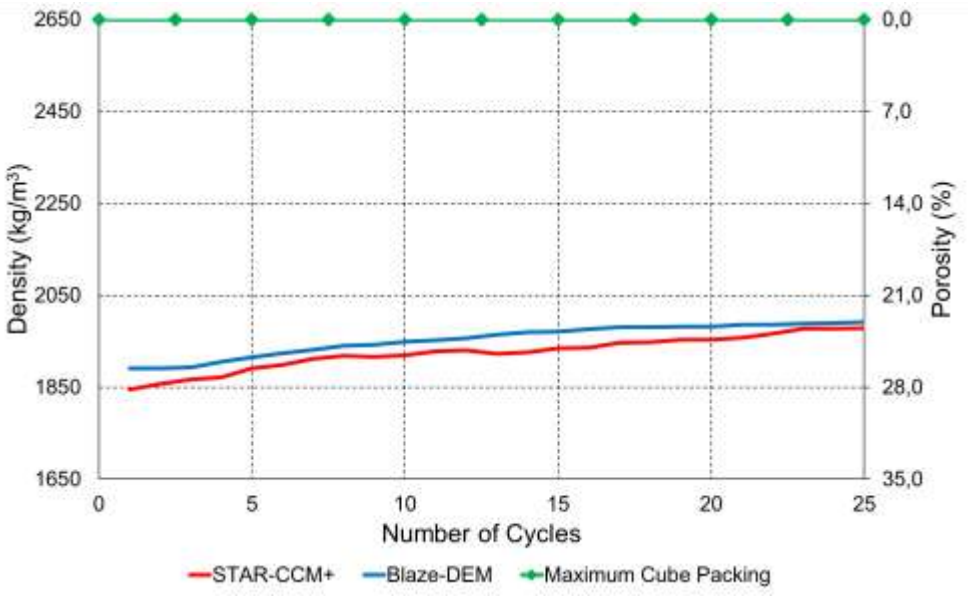

Fig. 11. Results of bulk density comparison from software suites considered

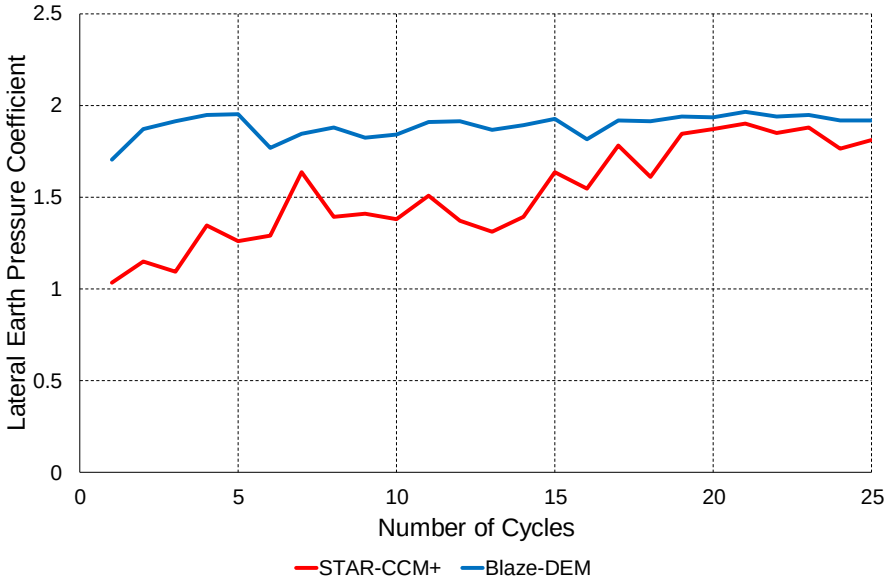

Fig. 12. Results of lateral earth pressure comparison from software suites considered

5. Results of DEM modelling

Using the six different particle shapes, a total of six simulations were performed in Blaze-DEM to study the effect of granular particle shape on the response of backfill retained by integral bridge abutments. For each of the simulations, the particles were injected from a grid at the top of the model and allowed to settle under only gravitational loads until a state of zero velocity was reached. The model abutment was then cyclically rotated 25 times in the passive and active directions as described in Section 3.2.

5.1. Bulk density distribution

The spatial density distributions in the granular backfill with distance away from the rotating wall were investigated for each of the particle shapes differing in sphericity. For this purpose, the area behind the model abutment was split into 8 zones of equal width as presented in Figure 13. Zone 1 represents the strip of backfill closest to the rotating model abutment, while Zone 8 refers to the strip furthest from the abutment.

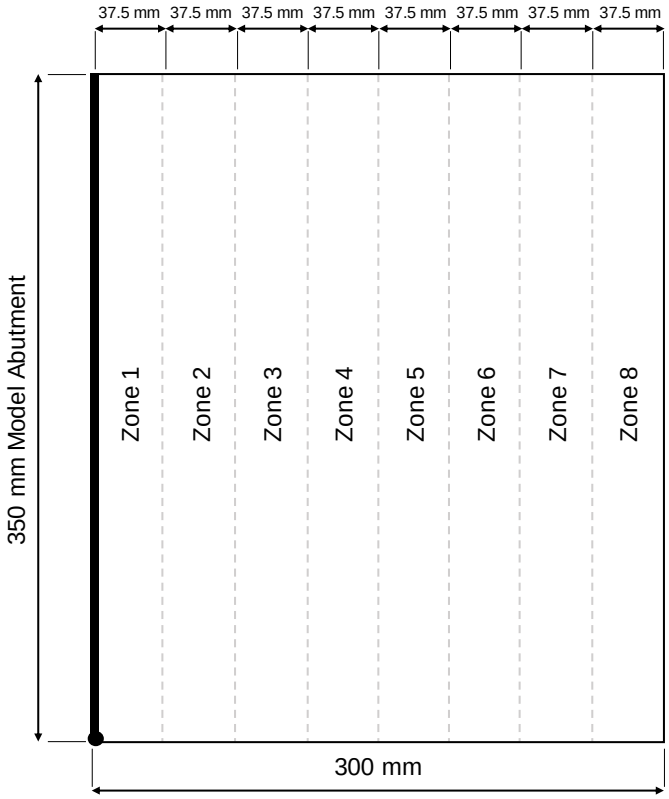

Fig. 13. Zones used for spatial density distribution

Figure 14 illustrates changes in the bulk density of the spheres, dodecahedrons, cubes and tetrahedrons during cyclic abutment displacement for the zones identified in Figure 13. The figure shows considerable densification during the first cycle, but that the rate of densification rapidly reduced thereafter. The results indicate that the particles with higher sphericities, specifically the spheres, experienced densifications over a larger domain. However, the particles with higher angularities experienced densification mainly restricted to the area close to the abutment. The result was that the spatial density distributions for the spheres were almost uniform across the 8 zones considered, while density distributions became more non-uniform with decreasing sphericity.

The differences in density between Zones 1 and 8 after 25 displacement cycles, expressed as a percentage, are compared to the sphericities of the various particles in Figure 15. The figure shows that the difference in densities reduced linearly with increasing sphericity.

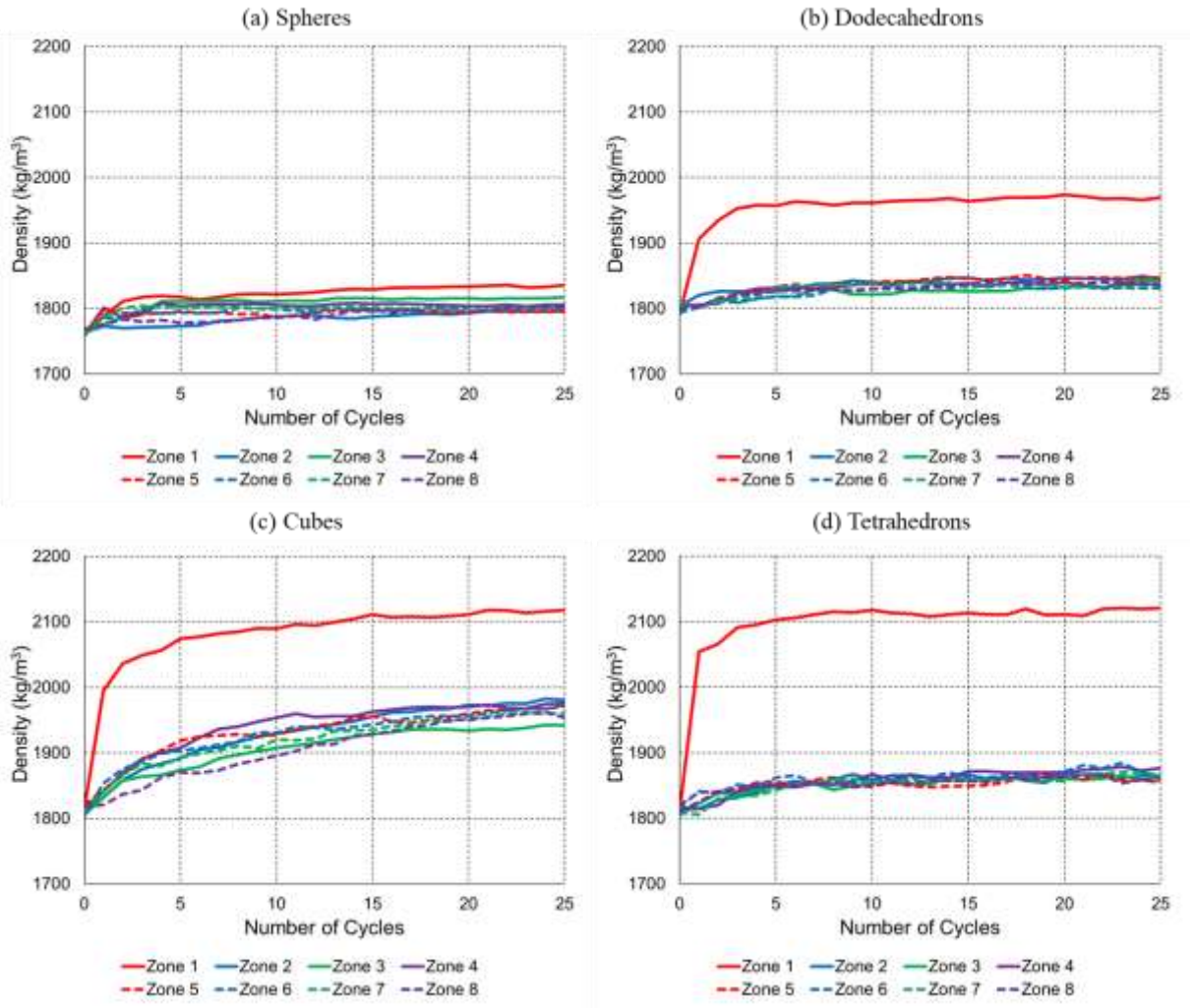

Fig. 14. Spatial density distributions for selected particle shapes

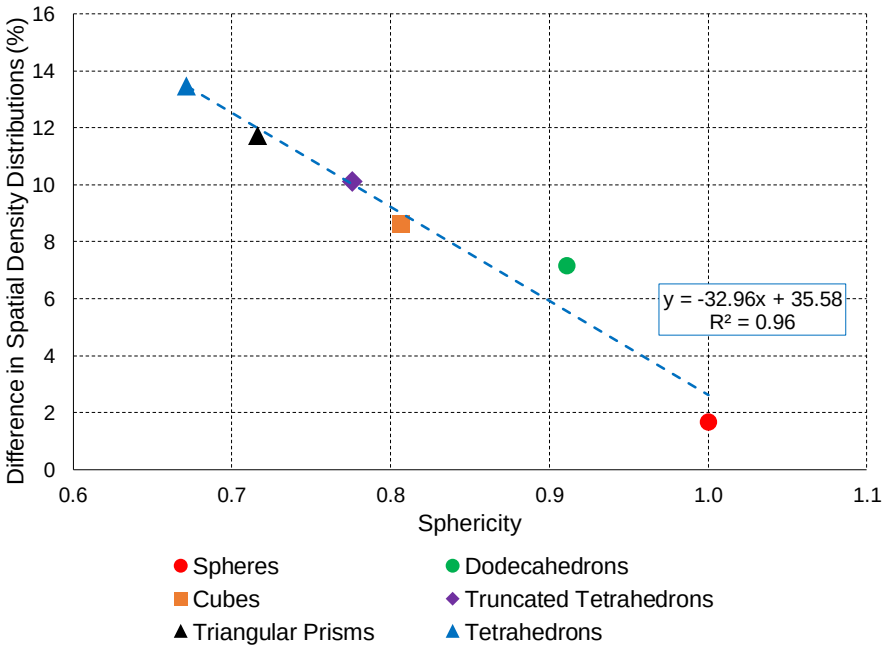

Fig. 15. Effect of particle sphericity on spatial density distribution difference after 25 cycles

5.2. Lateral earth pressure

The mobilised lateral earth pressure coefficients for the six particle shapes, calculated as explained in Section 4, are shown in Figure 16 against the number of displacement cycles. The figure shows that the shape of the particles influenced the lateral earth pressures mobilised on the model abutment as the abutment was cyclically rotated. This effect was studied by investigating the percentage increase in the average earth pressure coefficient per cycle for the different particle shape sphericities between the first cycle and the value after 25 cycles. Figure 17 illustrates the effect of sphericity on the percentage increase in the lateral earth pressure coefficients. The figure shows that for particle shapes with higher sphericities, the build-up of lateral earth pressure behind the model abutment was lower, while particle shapes with lower sphericities (higher angularities) had a greater build-up of lateral pressures. A linear relationship was observed between the particle shape sphericity and the increase in lateral earth pressure over the 25 displacement cycles.

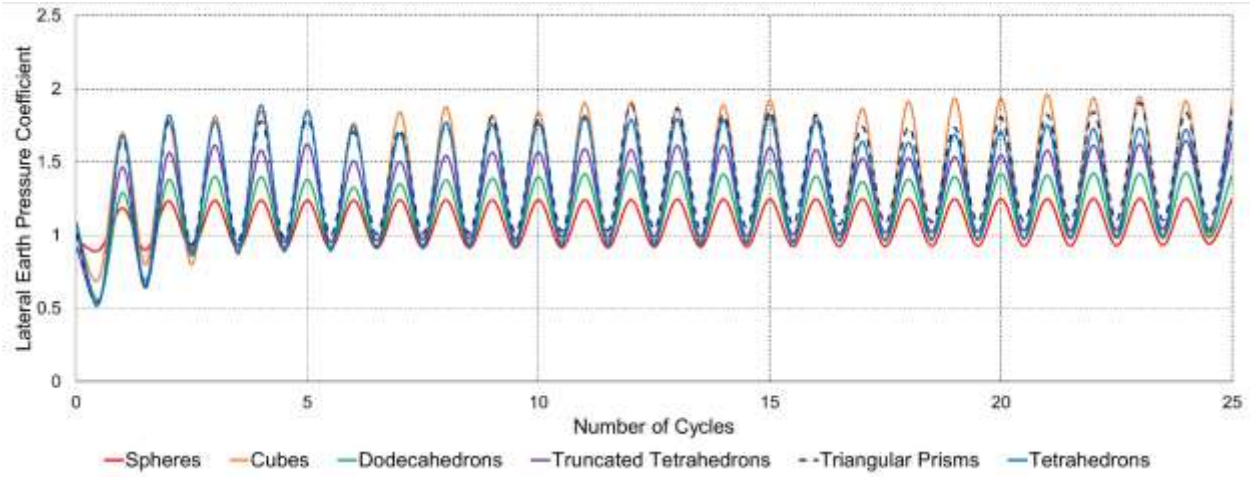

Fig. 16. Lateral earth pressure coefficients for various particle shapes

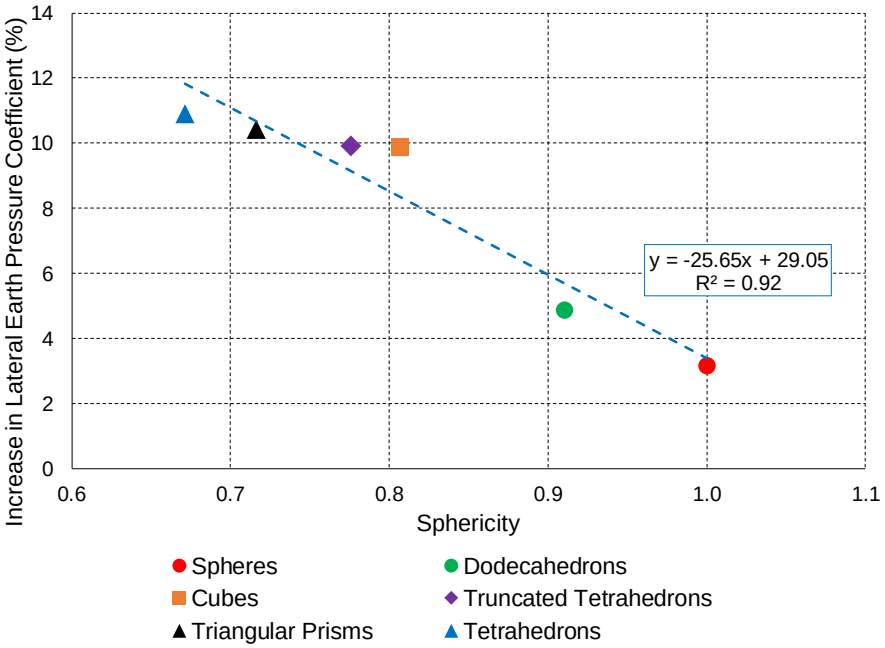

Fig. 17. Effect of particle sphericity on increase in lateral earth pressure coefficient over 25 displacement cycles

5.3. Particle rearrangement

Illustrations of the cubes from the first and last (25^{th}) cycles are shown in Figures 18 (a) and (b). The figures depict the packing of the cubes with a few key zones highlighted. Figure 18 (a) shows the particles with random orientations immediately after injection, i.e. before the abutment was cyclically rotated. Figure 18 (b) highlights a few locations where cubes which started with random orientations eventually re-orientated to become densely packed after a number of cycles to form intact groups of cubes acting as a unit. This change in packing structure resulted in a stiffer matrix in the backfill and is suggested to be one of the causes of the larger lateral stresses acting on the abutment with increasing cycles. In contrast to

densification, which occurred only near the rotating abutment for angular particles, the particle reorientation effects occurred over the entire domain behind the model abutment.

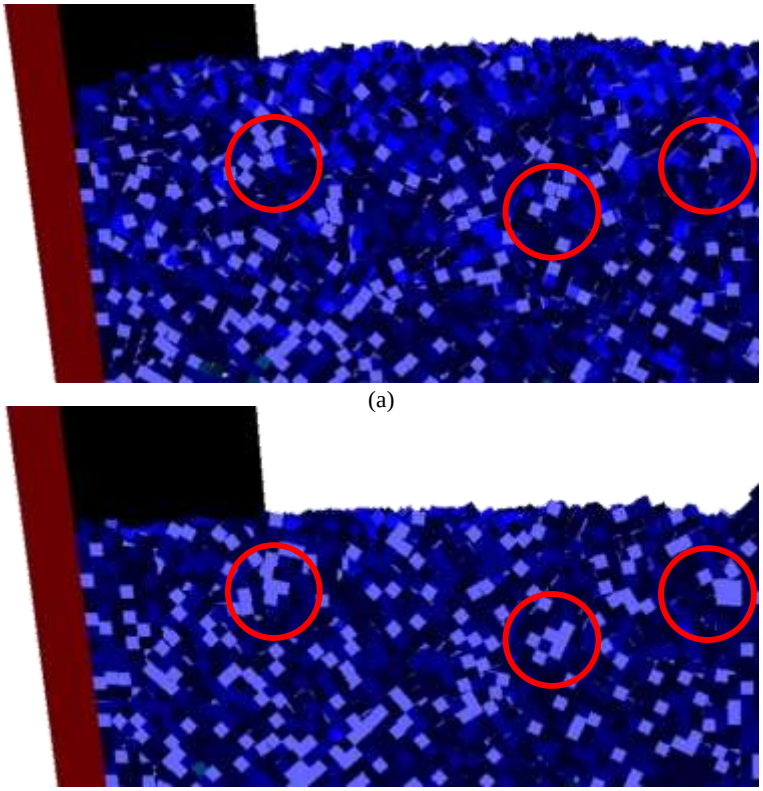

(a)

(b)

Fig. 18. Packing of cubes after: (a) first cycle and (b) last cycle (model abutment visible on the left)

Figure 19 presents histograms displaying the total particle reorientation for five particle shapes undergone between the first and the last abutment rotation cycles, arranged in order of decreasing particle sphericity. The particle reorientations for each of the eight zones identified in Figure 13 are indicated in different colours. In general, the histograms of particles reorientation do not vary much across the eight zones, plotting on each other. However, the cubes and tetrahedrons are exceptions. Cubes in contact with the left and right model boundaries were restricted from rotation because of full-face contact between the particles and the model boundary surfaces. This resulted in significantly smaller rotations in zones 1 and 8 compared to the inner zones (2 to 7). Some rotation restriction at the left and right model boundaries was also evident for the other less spherical particles, but to a lesser extent than for cubes. The more spherical dodecahedrons showed negligible spatial variation in rotation angle. Although not explicitly calculated, spheres are expected to behave similarly. The tetrahedrons, the most angular particles investigated, showed the greatest spatial variation in the rotation angle histograms, with somewhat smaller rotation angles occurring at the model boundaries. Rotation angles increased somewhat towards the centre of the model. The magnitude of the rotation angles were also the greatest in the case of the tetrahedrons, with mode values of approximately 7 to 8 degrees. Rotation angle mode values for the truncated tetrahedrons were around 6 to 7 degrees and approximately 4 to 6 degrees for the other particles, illustrating that particle reorientation generally reduced with increasing sphericity (reducing angularity).

Overall, the mode of the reorientation angles for the different particles investigated fell in a narrow range (4 to 7 degrees), although rotation angles varied over a wide range as shown by the histograms. The range in rotation angles (total width of the histograms) seemed to reduce somewhat with reducing sphericity (increasing angularity).

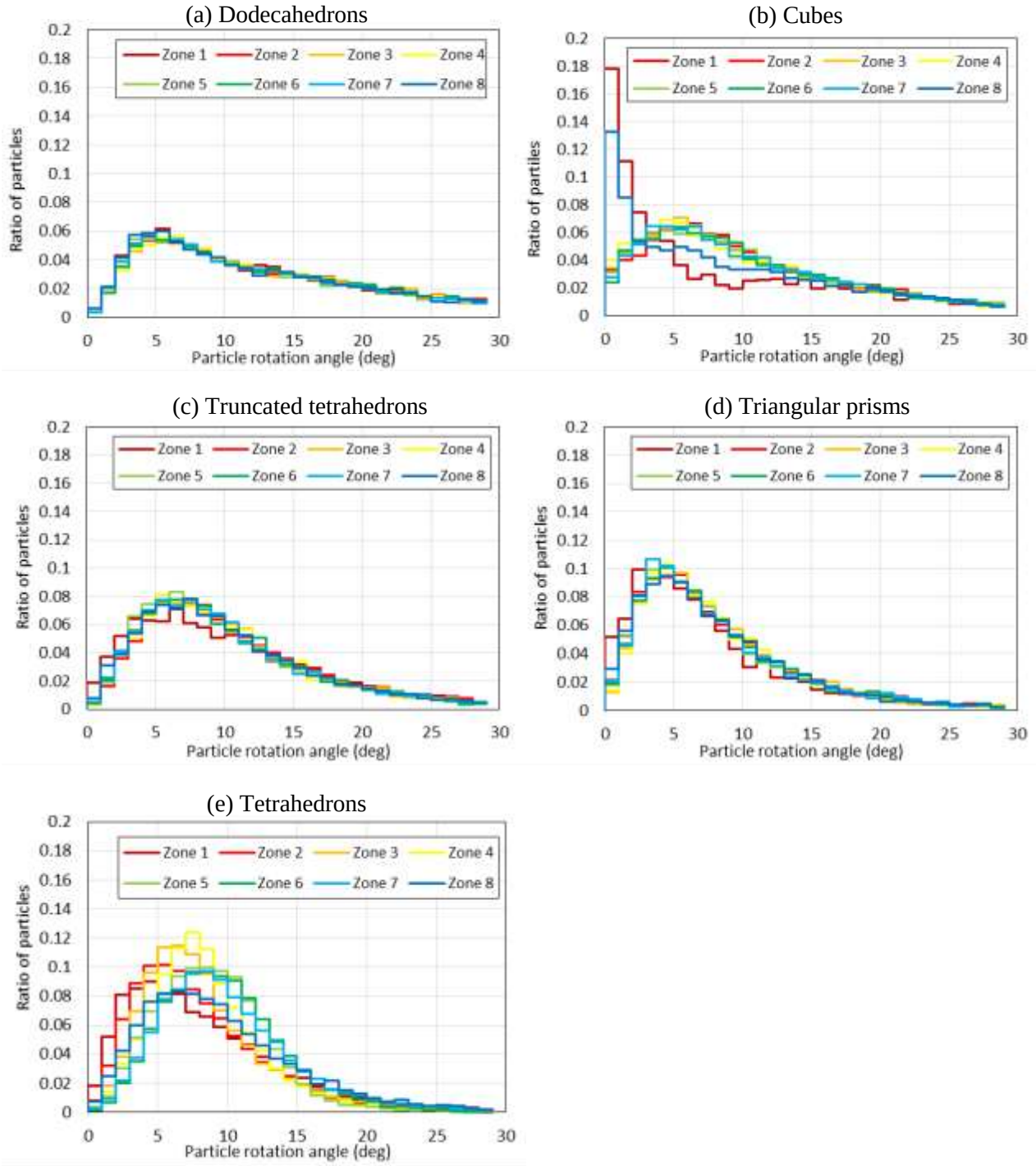

Fig. 19. Histograms of particle reorientation for (a) dodecahedrons, (b) cubes, (c) truncated tetrahedrons, (d) triangular prisms and (e) tetrahedrons

5.4. *Discussion*

The results of the simulations in Blaze-DEM indicate that backfill particle sphericity plays a significant role in the build-up of stresses acting on a cyclically displaced integral bridge abutment. Particle shapes with lower sphericities (spheres and dodecahedrons) experienced lower build-ups of stress as opposed to the more angular shapes, such as the tetrahedrons and triangular prisms. This is similar to observations by Clayton *et al.* [1] and Xu *et al.* [3]. Particle shapes of higher sphericities experienced densification over larger domains, while particle shapes with higher angularities primarily underwent reorientation, somewhat restricted due to full-face contact at the model boundaries, increasing towards the centre.

The localised movements and reorientation observed with the particle shapes of lower sphericities (i.e. high angularity) is suggested to be one of the reasons for the differences in the amount and rate of stress build-up between the particle shapes. These localised particle movements allowed greater interlocking mechanisms to develop, resulting in a stiffer particulate mass, supporting the larger stress accumulations observed with the particle shapes of lower sphericities. The reduced accumulation of stresses observed with the particle shapes with higher sphericities is suggested to be a result primarily of densification.

The observations support recommendations contained in texts on integral bridge design [6,7] that place a limit on the strength of the material used as backfill behind integral bridge abutments. Results illustrate how lateral earth pressures can be limited by using uniform sand particles of high sphericity as recommended by the abovementioned sources. Soils comprising of particles of high sphericity are likely to have a lower shear strength than soils comprising of angular particles which will support greater degrees of interlock and hence greater lateral stress. Figure 17 may provide an indication of the sensitivity of the cyclic lateral earth pressure magnitude on the degree of sphericity of the particles comprising the backfill (subject to the cycling deformations imposed in this study).

Using Blaze-DEM to perform the simulations modelling spheres and the five convex polyhedra analysed, provided much shorter computational times compared to what can be achieved using conventional CPU based software. The comparison of selected results between the two programs, investigating the response of cubes, confirms that Blaze-DEM delivered results of which compares well with that of STAR-CCM+ in terms of particle densification and lateral earth pressure response behind the rotating abutment after several cycles

6. Conclusions and recommendations

The discrete element method was used within a research code, Blaze-DEM, to investigate the effect of granular particle shape on the response of backfill material retained by integral bridge abutments. Aspects of response investigated were densification, lateral stress changes and particle reorientation behind the abutment during displacement cycles. The backfill was subjected to simulated cyclic thermal-induced displacements of a model integral bridge abutment. The shapes modelled included spheres and the following convex polyhedral shapes: dodecahedrons, truncated tetrahedrons, tetrahedrons, triangular prisms and cubes.

A software comparison was performed between Blaze-DEM and the commercial code, STAR-CCM+ to verify the performance of Blaze-DEM. The primary differences between the software suites are the computing hardware utilised and the particle shapes which can be modelled. STAR-CCM+ makes use of the central processing unit (CPU) and is restricted to modelling spheres, sphere-clumped shapes and convex

polyhedra. Blaze-DEM uses a graphics processing unit (GPU) and has the ability to model spherical, as well as convex and non-convex polyhedra.

The results from the software comparison showed that Blaze-DEM offers comparable results to STAR-CCM+. However, using the GPU to perform DEM simulations resulted in an elevated level of performance and it was found that Blaze-DEM could offer computational times over 150 times faster for the equivalent simulation in STAR-CCM+. This two order of magnitude increase in computational ability and the less restricted particle shape modelling capabilities enable parametric studies of geotechnical engineering problems to be performed using DEM simulation in more reasonable time frames.

The results from the investigation showed that the rate and magnitude of horizontal stress build-up during cyclic abutment displacement were strongly related to particle sphericity. The stress build-up in backfill comprising of particles of high sphericity was gradual and related to densification, which extended over the entire backfill domain modelled behind the abutment. As sphericity reduced, i.e. with increasing angularity, densification became more localised to the area near the abutment, but larger and more rapid lateral stress build-up occurred during displacement cycles. The larger lateral stress accumulation observed with shapes of higher angularity is suggested to be a result of not only localised densification, but also a result of the evolution of structure within the particulate mass due to particle interlocking and reorientation. This resulted in a stiffer particle mass, not only in the zone of densification, but also further away. Following recommendations that the shear strength of backfill behind integral bridge abutments should be limited [6,7], the DEM analyses suggest the use of backfill comprising of particles of high sphericity.

Potential future work involves modelling the response of non-convex polyhedral particles. These particle shapes are expected to enable greater degrees of reorientation and interlocking between the particles, hence an enhanced development of structure, which could possibly result in a larger build-up of stress when compared to the spherical and convex polyhedral shapes [30].

References

[1] Clayton CRI, Xu M, Bloodworth A. A laboratory study of the development of earth pressure behind integral bridge abutments. Géotechnique 2006;56:561–71. doi:10.1680/geot.2006.56.8.561.

[2] Bloodworth AG, Xu M, Banks JR, Clayton CRI. Predicting the Earth on Integral Bridge Abutments. J Bridg Eng 2011;16:259–66. doi:10.1061/(ASCE)BE.1943-5592.

[3] Xu M, Clayton CR, Bloodworth AG. The earth pressure behind full-height frame integral abutments supporting granular fill. Can Geotech J 2007;44:284–98. doi:10.1139/t06-122.

[4] Biddle, A. R., Iles, D. C. Yandzio ED. Integral steel bridges: Design guidance. 1997.

[5] Ng C, Springman S, Norrish A. Soil-structure interaction of spread-base integral bridge abutments. Soils Found 1998;38:145–62. doi:10.1061/(ASCE)1090-0241(1998)124:5(376).

[6] Collings D. Steel Concrete Composite Bridges 2005. doi:10.1680/sccb.33429.

[7] The Highways Agency. The Design of Integral Bridges. Des Man Des Road Bridg 2003;1.

[8] Cundall PA, Strack ODL. A discrete numerical model for granular assemblies. Géotechnique 1979;29:47–65. doi:10.1680/geot.1979.29.1.47.

[9] Höhner D, Wirtz S, Scherer V. A study on the influence of particle shape and shape approximation on particle mechanics in a rotating drum using the discrete element method. Powder Technol 2014;253:256–65. doi:10.1016/j.powtec.2013.11.023.

[10] Govender N, Wilke DN, Kok S, Els R. Development of a convex polyhedral discrete element simulation framework for NVIDIA Kepler based GPUs. J Comput Appl Math 2014;270:386–400. doi:10.1016/j.cam.2013.12.032.

[11] Cleary PW, Sawley ML. DEM modelling of industrial granular flows: 3D case studies and the effect of particle shape on hopper discharge. Appl Math Model 2002;26:89–111.

doi:10.1016/S0307-904X(01)00050-6.
[12] Fu R, Hu X, Zhou B. Discrete element modeling of crushable sands considering realistic particle shape effect. Comput Geotech 2017;91:179–91. doi:10.1016/j.compgeo.2017.07.016.
[13] Govender N. Blaze-DEM: A GPU based large scale 3D discrete element particle transport framework. University of Pretoria, 2015.
[14] Govender N, Wilke DN, Pizette P, Abriak NE. A study of shape non-uniformity and poly-dispersity in hopper discharge of spherical and polyhedral particle systems using the Blaze-DEM GPU code. Appl Math Comput 2018;319:318–36. doi:10.1016/j.amc.2017.03.037.
[15] Govender N, Wilke DN, Kok S. Collision detection of convex polyhedra on the NVIDIA GPU architecture for the discrete element method. Appl Math Comput 2015;267:810–29. doi:10.1016/j.amc.2014.10.013.
[16] Govender N, Rajamani RK, Kok S, Wilke DN. Discrete element simulation of mill charge in 3D using the BLAZE-DEM GPU framework. Miner Eng 2015;79:152–68. doi:10.1016/j.mineng.2015.05.010.
[17] Siemens Product Lifecycle Management Software Inc. STAR-CCM+ 2017.
[18] Skorpen, S., Kearsley, E., Clayton, C. Kruger E. The Initial Environmental Effects on the Design of a 90m Long Integral Bridge in South Africa. FIB Symp. 2016 Performance-Based Approaches Concr. Struct., 2016.
[19] Roeder C. Proposed Design Method for Thermal Bridge Movements. J Bridg Eng 2003;8:12–9.
[20] Coetzee CJ. Calibration of the discrete element method and the effect of particle shape. Powder Technol 2016;297:50–70. doi:10.1016/j.powtec.2016.04.003.
[21] Wadell H. Volume, Shape, and Roundness of Quartz Particles. J Geol 1935;43:250–80. doi:10.1086/624298.
[22] Coetzee CJ. Review: Calibration of the discrete element method. Powder Technol 2017;310:104–42. doi:10.1016/j.powtec.2017.01.015.
[23] Xu Y, Kafui KD, Thornton C, Lian G. Effects of material properties on granular flow in a silo using DEM simulation. Part Sci Technol 2002;20:109–24. doi:10.1080/02726350215338.
[24] Chang YL, Chen TH, Weng MC. Modeling particle rolling behavior by the modified eccentric circle model of DEM. Rock Mech Rock Eng 2012;45:851–62. doi:10.1007/s00603-012-0227-0.
[25] Tu X, Andrade JE. Criteria for static equilibrium in particulate mechanics computations. Int J Numer Methods Eng 2008;75:1581–606. doi:10.1002/nme.2322.
[26] Sandlin MJ. An Experimental and Numerical Study of Granular Hopper Flows 2013.
[27] Härtl J, Ooi JY. Experiments and simulations of direct shear tests: Porosity, contact friction and bulk friction. Granul Matter 2008;10:263–71. doi:10.1007/s10035-008-0085-3.
[28] Govender N, Wilke DN, Kok S. Blaze-DEMGPU: Modular high performance DEM framework for the GPU architecture. SoftwareX 2015;5:62–6. doi:10.1016/j.softx.2016.04.004.
[29] Kelesoglu MK, Springman SM. Analytical and 3D numerical modelling of full-height bridge abutments constructed on pile foundations through soft soils. Comput Geotech 2011;38:934–48. doi:10.1016/j.compgeo.2011.07.011.
[30] Wilke DN, Govender N, Pizette P, Abriak NE. Computing with non-convex polyhedra on the GPU. Springer Proc. Phys., vol. 188, 2017, p. 1371–7. doi:10.1007/978-981-10-1926-5_141.